Molecular Recognition Directed Self-assembly of Supramolecular Cylindrical Channel-like Architectures from 6,7,9,10,12,13,15,16-Octahydro-1,4,7,10,13-pentaoxabenzocyclopentadecen-2-ylmethyl 3,4,5-Tris(*p*-dodecyloxybenzyloxy)benzoate

Virgil Percec,*[a] Gary Johansson,[a] James Heck,[a] Goran Ungar[b] and Simon V. Batty[b]
[a] *Department of Macromolecular Science, Case Western Reserve University, Cleveland, OH 44106, USA*
[b] *School of Materials, The University of Sheffield, Sheffield, S1 3JD, UK*

Complexation of the crown ether receptor of the benzo-15-crown-5 benzoate **6** [6,7,9,10,12,13,15,16-octahydro-1,4,7,10,13-pentaoxabenzocyclopentadecen-2-ylmethyl 3,4,5-tris(*p*-dodecyloxybenzyloxy)benzoate] **6** with $NaCF_3SO_3$ and KCF_3SO_3 destabilizes the crystalline phase of **6** and induces the self-assembly of a supramolecular cylindrical channel-like architecture which displays an enantiotropic thermotropic disordered hexagonal columnar (Φ_h) mesophase. Characterization of this supramolecular architecture was performed by a combination of differential scanning calorimetry (DSC), X-ray scattering, thermal optical polarized microscopy, DC conductivity and molecular modelling. A model is proposed in which a stratum of the column is formed by *ca.* 5.8 molecules of **6** with their benzo-15-crown-5 receptors placed side-by-side in the centre of the column and their melted alkyl tails radiating towards its periphery. *endo*-Recognition generated *via* the benzo-15-crown-5 receptor upon complexation, and *exo*-recognition provided by the tapered 3,4,5-tris(*p*-dodecyloxybenzyloxy)benzoate fragment of **6** (most probably functioning *via* hydrophobic–hydrophobic interactions) provide the driving force for the self-assembly of this channel-like supramolecule. This mechanism of self-assembly resembles that of tobacco mosaic virus (TMV).

For the past 150 years organic chemists have been concerned with the understanding of the covalent bond. Recently, research on molecular recognition (generated by weak noncovalent interactions) has been recognized world wide as an important intellectual and technological frontier.[1] *endo*- (Generated by convergent cavities) and *exo*- (generated by larger bodies of similar size and shapes, or surfaces) molecular recognition,[2] preorganization, and self-organization provide the basis of spontaneous generation of functional supramolecular architectures *via* self-assembly from their components.[3] Molecular-recognition directed organic synthesis,[4] and self-assembly of supramolecular architectures[2-4] are two of the most active topics of supramolecular chemistry.[2a]

It is widely accepted that molecular recognition-directed synthesis and self-assembly are responsible for the generation and the fascinating properties of biological systems. Ionic channels, which are responsible for selective transport in many natural processes, are generated and function *via* these principles.[5] Gramicidin A is the best understood natural cation conducting ionic channel. It is generated in phospholipid membranes and is selective for monovalent cations.[5f,6] Gramicidin A consists of two hydrophilic polypeptide chains which either exist as a double helix in solution (pore conformation) or as an end-to-end helical shape in the membrane bound form (channel conformation). In the tunnel shaped conformation, its hydrophobic groups are turned outward and the carbonyl groups are turned inward. The cation, probably in partially hydrated form, moves *via* carbonyl groups from entrance to exit. The conformation and the central cavity diameter of gramicidin A are determined by the type and, therefore, the size of cation complexed.

Several different routes were elaborated for the molecular design of synthetic ionic channels. Some of them were reviewed.[5f] They can be briefly classified as follows: (*a*) isomorphic systems based on cryptands, crown ethers and azacrown ethers,[7a-f] β-cyclodextrin,[7g] and acyclic polymers[7h] and oligomers[7i] as *endo*-receptors; (*b*) microphase separated membranes based on mixtures of polymers, low-molar mass liquid crystals, and crown ethers;[8] (*c*) thermotropic low molar mass[9a-d] and polymeric liquid crystals containing crown ethers and rod-like mesogens;[9e-k] (*d*) azamacrocyclic derivatives exhibiting thermotropic columnar hexagonal mesophases;[10] and (*e*) phthalocyanines containing crown ethers and exhibiting columnar hexagonal mesophases.[11]

Recently, we have demonstrated the manipulation of reversible phase transitions of thermotropic side-chain liquid-crystalline polymers containing crown ethers *via* molecular recognition.[9k] The induction of a columnar hexagonal (Φ_h) mesophase in a substituted azamacrocyclic derivative *via* complexation with metal salts was also reported.[10b] In both cases it has been suggested that the manipulation of the phase transitions *via* complexation is due to a combination of enhanced rigidity of the complexed receptor and ionic interactions between complexed and uncomplexed receptors.[9k,10b]

This paper reports a novel approach to the design of ionic channel-like supramolecular architectures. This is based on molecular recognition-directed self-assembly of a supramolecular architecture exhibiting a columnar hexagonal mesophase which resembles an ionic channel. The particular example described here refers to the self-assembly of an enantiotropic thermotropic disordered columnar hexagonal phase (Φ_h) from 6,7,9,10,12,13,15,16-octahydro-1,4,7,10,13-pentaoxabenzocyclopentadecen-2-ylmethyl 3,4,5-tris(*p*-dodecyloxybenzyloxy)benzoate **6** *via* complexation with sodium and potassium triflates. Compound **6** contains the benzo-15-crown-5 group which acts as an *endo*-receptor and the 3,4,5-tris(*p*-dodecyloxybenzyloxy)benzoate tapered moiety which plays the role of exo-receptor. The self-assembly of **6** takes place *via* a combination of *endo*- and *exo*-recognition.

Previous examples of liquid crystalline compounds containing crown ethers had the crown ether receptor placed either at one end of the monomeric[9a-d] or polymeric[9e-k] rigid rod-like mesogenic group which exhibited calamitic mesophases, or on the periphery of the column which generated the columnar

hexagonal mesophase.[11] To our knowledge the example described here is the first one in which the crown ether receptor is located within the centre of the column. The only other examples of supramolecular systems exhibiting a thermotropic columnar hexagonal (Φ_h) mesophase and containing an *endo*-receptor located within the centre of the column are all based on substituted azamacrocyclics.[10]

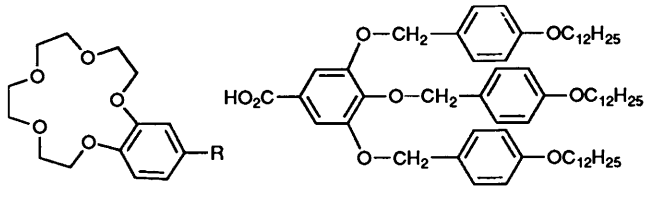

i 1 R = H
ii 2 R = Ac
iii 3 R = CO_2H
iv 4 R = CH_2OH
6 R = $CH_2OCOC_6H_2(OCH_2C_6H_4OC_{12}H_{25}$-*p*$)_3$-3,4,5

Scheme 1 *Reagents and conditions:* i, Ac_2O, AcOH, PPA, 70 °C; ii, NaOH, 0 °C; iii, H_3B·THF, room temp.; iv, compound **5**, DCC, DPTS, CH_2Cl_2 room temp.

Experimental

Materials.—Trifluoromethanesulfonic acid (98%), picric acid (A.C.S. reagent, containing 35% water), borane–tetrahydrofuran complex (1.0 mol dm^{-3} solution in tetrahydrofuran), tetrabutylammonium hydrogen sulfate (TBAH) (97%), toluene-*p*-sulfonyl chloride (*p*-TsCl) (98%), dicyclohexylcarbodiimide (DCC) (99%), toluene-*p*-sulfonic acid monohydrate (98%) (all from Aldrich), potassium carbonate (reagent grade, Fisher), and 4-dimethylaminopyridine (99%, Lancaster) were used as received. Tetrahydrofuran (THF) (Fisher) was refluxed over sodium with benzophenone until the solution turned purple, then was freshly distilled before use. Methylene dichloride (CH_2Cl_2) and 1,2-dichloroethane (reagent grade, Fisher) were refluxed over CaH_2 and distilled before use. 4-Dimethylaminopyridinium toluene-*p*-sulfonate (DPTS) was prepared according to a literature procedure.[12] Water of hydration was removed from toluene-*p*-sulfonic acid by azeotropic distillation with benzene. Addition of a stoichiometric amount of 4-dimethylaminopyridine in warm benzene precipitated the pyridinium salt. The white solid, collected by vacuum filtration, was recrystallized from 1,2-dichloroethane to give DPTS as white needles, m.p. 170–172 °C (lit.,[12] m.p. 165 °C). Sodium and potassium triflate were prepared by the vacuum distillation of trifluoromethanesulfonic acid (5 cm^3) into a receiving flask charged with the appropriate chloride salt (MCl, M = Na or K). After the mixture had been heated at 60 °C for 1 h, the salt was filtered off, washed with diethyl ether and dried *in vacuo* to give the pure triflate salt: M = Na, m.p. 247–249 °C (lit.,[13] m.p. 248 °C) and M = K, m.p. 234–236 °C (lit.,[13] m.p. 230 °C).

Techniques.—^{1}H NMR (200 MHz) spectra were recorded on a Varian XL 200 spectrometer with tetramethylsilane (TMS) as internal standard; *J*-values are given in Hz. IR spectra were recorded on a Perkin-Elmer 1320 IR spectrometer. The purity of products was determined by a combination of thin layer chromatography (TLC) on silica gel plates (Kodak) with fluorescent indicator and high pressure liquid chromatography (HPLC) using a Perkin-Elmer Series 10 high-pressure liquid chromatograph equipped with an LC-100 column oven, Nelson Analytical 900 Series integrator data station, and two Perkin-Elmer PL gel columns of 5 × 10^2 and 1 × 10^4 Å. $CHCl_3$ was used as solvent at the oven temperature of 40 °C. Detection was by UV absorbance at 254 nm. Thermal transitions were measured on a Perkin-Elmer DSC-4 differential scanning calorimeter (DSC) equipped with a TADS data station. In all cases, the heating and cooling rates were 20 °C min^{-1}. The transition temperatures were reported as the maxima and minima of their endothermic and exothermic peaks. Glass transition temperatures (T_g) were read at the middle of the change in heat capacity. Indium was used as calibration standard. X-Ray scattering patterns were recorded using either a helium-filled wide-angle flat plate (WAXS) camera or a pinhole-collimated small-angle (SAXS) camera. Ni-filtered Cu-Kα radiation was used. The temperature stability of the X-ray heating cell was ±0.1 °C. A Carl-Zeiss optical polarized microscope (100 × magnification) equipped with a Mettler FP 82 hot stage and a Mettler FP 80 central processor was used to verify thermal transitions and characterize anisotropic textures. Molecular modelling was done using the computer program CSC Chem3D™ from Cambridge Scientific Computing, Inc. DC conductivity of the complex of **6** with $NaCF_3SO_3$ (0.6 mol) (**6**-0.6) was measured using a two-point probe with a guard ring to intercept surface current. The sample was in the form of a 2 mm thick cylindrical pressed pellet of 13 mm diameter. The design of the cell was such that the geometry between the electrodes was fixed and independent of the physical state of the sample. A Keithley instrument was employed, and the cell was evacuated. Prior to measurements the sample was kept in a vacuum dessicator for several days. Heating and cooling temperature sweeps were performed at a rate of 1 to 2 °C min^{-1}.

Scheme 1 outlines the synthesis of the benzo-15-crown-5 benzoate **6**.

6,7,9,10,12,13,15,16-*Octahydro*-1,4,7,10,13-*pentaoxabenzocyclopentadecene* (*Benzo*-15-*crown*-5) **1**.—The title compound **1**, synthesized from pyrocatechol and 1,11-dichloro-3,6,9-trioxaundecane according to a literature method,[14] was obtained in 54% yield (purity 97.8% by HPLC); m.p. 76–78 °C (lit.,[14] m.p. 78–80 °C); δ_H($CDCl_3$, TMS) 3.77 (m, 8 H, OCH_2CH_2O-), 3.92 (m, 4 H, -$PhOCH_2CH_2$), 4.12 (m, 4 H, -$PhOCH_2CH_2$) and 6.90 (s, 4 H, ArH).

2-*Acetyl*-6,7,9,10,12,13,15,16-*octahydro*-1,4,7,10,13-*pentaoxabenzocyclopentadecene* **2**.—The title compound **2**, synthesized by the acylation of **1** with acetic acid in polyphosphoric acid,[9i,15] was obtained in 86% yield; m.p. 94–95 °C (lit.,[15b] m.p. 95.5–96.5 °C); δ_H($CDCl_3$, TMS) 2.56 (s, 3 H, CH_3CO), 3.77 (s, 8 H, OCH_2CH_2O), 3.93 (m, 4 H, $ArOCH_2CH_2O$), 4.20 (m, 4 H, $ArOCH_2CH_2O$), 6.89 (d, 1 H, *meta* to Ac on aromatic ring, *J* 8.2), 7.59 (s, 1 H, *ortho* to Ac on aromatic ring), 7.60 (d, 1 H, *ortho* to Ac on aromatic ring, *J* 8.4).

6,7,9,10,12,13,15,16-*Octahydro*-1,4,7,10,13-*Pentaoxabenzocyclopentadecene*-2-*carboxylic Acid* **3**.—The title compound **3**, synthesized by the oxidation of **2** with sodium hypobromite,[9i,16] was obtained in 83% yield; m.p. 185–186 °C (lit.,[16] m.p. 180 °C); δ_H($CDCl_3$, TMS) 3.77 (s, 8 H, OCH_2CH_2O), 3.92 (m, 4 H, $ArOCH_2CH_2O$), 4.18 (m, 4 H, $ArOCH_2CH_2O$), 6.89 (d, 1 H, *meta* to CO_2H, on aromatic ring, *J* 8.0), 7.56 (s, 1 H, *ortho* to CO_2H on aromatic ring), 7.69 (d, 1 H, *ortho* to CO_2H on aromatic ring, *J* 8.0) and 12.25 (s, 1 H, CO_2H).

2-*Hydroxymethyl*-6,7,9,10,12,13,15,16-*octahydro*-1,4,7,10,13-*pentaoxabenzocyclopentadecene* **4**.—Following a literature procedure,[17] the acid **3** (7.55 g, 24.2 mmol) was added to dry THF (275 cm^3) at room temperature in a round-bottom flask equipped with a magnetic stirrer, dropping funnel, and nitrogen inlet–outlet. Borane–THF (32.2 cm^3, 32.2 mmol) was added dropwise to the heterogeneous mixture which was then stirred for 3 h at room temperature. After excess of borane had been decomposed by slow addition of a THF–H_2O solution (1:1; 30

cm^3), the mixture was poured into a separatory funnel and washed with saturated aqueous potassium carbonate (100 cm^3). The organic layer was dried ($MgSO_4$), filtered, and evaporated on a rotary evaporator. Recrystallization of the residue from cold (0 °C) light petroleum–propan-2-ol (1:1, v/v) gave a white solid (4.7 g, 65.1%), m.p. 45–47 °C (lit.,[18] m.p. 52–54 °C); δ_H($CDCl_3$, TMS) 2.74 (br s, 1 H, $HOCH_2$), 3.73 (m, 8 H, OCH_2CH_2O), 3.88 (m, 4 H, $ArOCH_2CH_2$), 4.08 (m, 4 H, $ArOCH_2CH_2$), 4.56 (s, 2 H, $HOCH_2$) and 6.82 (m, 3 H, ArH).

3,4,5-*Tris*[p-(*dodecyloxy*)*benzyloxy*]*benzoic Acid* **5**.—Compound **5**, the synthesis and purification of which have been reported previously,[19] was obtained 99% pure (HPLC). Thermal transition temperatures (°C) and enthalpy changes of the transitions (kcal mol^{-1}) are: *k* 49 (1.27) *k* 73 (14.17) Φ_h 147 (3.01) *i* on heating; *i* 137 (3.01) Φ_h 51.41 (6.89, overlapped peaks) *k* 9 (0.58) *k* on cooling (DSC, 20 °C min^{-1}); δ_H($CDCl_3$, TMS) 0.88 (t, 9 H, CH_3), 1.27 [m, 54 H, $(CH_2)_9$], 1.79 (m, 6 H, $C_6H_4OCH_2CH_2$), 3.97 (overlapped t, 6 H, $C_6H_4OCH_2CH_2$), 5.03 (s, 2 H, $OC_6H_4CH_2OC_6H_2CO_2$ from 4 position), 5.06 (s, 4 H, $OC_6H_4CH_2OC_6H_2CO_2$ from 3 and 5 positions), 6.76 (d, 2 H, *ortho* to oxygen on internal benzyl ring, *J* 8.9), 6.90 (d, 4 H, *ortho* to oxygen of external benzyl rings, *J* 8.4), 7.26 (d, 2 H, *meta* to oxygen of internal benzyl ring, *J* 8.3), 7.34 (d, 4 H, *meta* to oxygen of external benzyl rings, *J* 8.7) and 7.43 (s, 2 H, *ortho* to CO_2H); ν_{max}/cm^{-1} (KBr plate) 1690 (C=O).

6,7,9,10,12,13,15,16-*Octahydro*-1,4,7,10,13-*pentaoxabenzocyclopentadecene*-2-*ylmethyl* 3,4,5-*Tris*(p-*dodecyloxybenzyloxy*)*benzoate* **6**.—Compound **6** was synthesized as follows by a literature procedure.[12] Compounds **5** (1.0 g, 1.0 mmol) and **4** (0.31 g, 1.0 mmol) were dissolved in dry CH_2Cl_2 (5 cm^3) in a round bottom flask equipped with a magnetic stirrer. To this solution was added 4-dimethylaminopyridinium toluene-*p*-sulfonate (DPTS) (0.059 g, 0.20 mmol) and 1,3-dicyclohexylcarbodiimide (DCC) (0.27 g, 1.3 mmol). The mixture was stirred for 2 h at room temperature after which time the reaction was shown to be complete by ^1H NMR analysis. The mixture was filtered and the filtrate added to methanol to precipitate the product. The latter was collected by vacuum filtration and recrystallized from propan-2-ol–methanol (1:1) to yield a white powder (1.1 g, 85%); purity: 99% (HPLC); m.p. 94 °C (DSC, 20 °C min^{-1}); δ_H($CDCl_3$, TMS) 0.84 (t, 9 H, CH_3), 1.27 [m, 54 H, $(CH_2)_9$], 1.70 (m, 6 H, CH_2CH_2O), 3.76 (s, 8 H, OCH_2CH_2O), 3.89 (m, 4 H, $C_6H_3OCH_2CH_2O$), 3.95 (overlapped t, 6 H, $C_6H_4OCH_2CH_2$), 4.11 (m, 4 H, $C_6H_4OCH_2CH_2O$), 4.99 (s, 2 H, $OC_6H_4CH_2OC_6H_2CO_2$ from 4 position), 5.03 (s, 2 H, $OC_6H_4CH_2OC_6H_2CO_2$ from 3 and 5 positions), 5.24 (s, 2 H, $C_6H_2CO_2CH_2C_6H_3$), 6.77 (d, 2 H, *ortho* to oxygen of internal benzyl ring, *J* 8.8), 6.90 (d, 4 H, *ortho* to oxygen of external benzyl rings, *J* 8.7), 6.90–6.96 (overlapped peaks, 3 H, aromatic crown protons), 7.26 (d, 2 H, *meta* to oxygen of internal benzyl ring, *J* 8.6), 7.30 (d, 4 H, *meta* to oxygen of external benzyl rings, *J* 8.7) and 7.38 (s, 2 H, *ortho* to CO_2).

Preparation of Complexes of **6**.—Complexes of **6** with sodium triflate and potassium triflate were prepared by mixing solutions of **6** (*ca.* 20 mg cm^{-3}) in dry CH_2Cl_2 with an appropriate volume of 0.05 mol dm^{-3} salt in dry THF solution, followed by slow evaporation of the solvent under reduced pressure at room temperature and subsequent drying in a vacuum oven at 60 °C to constant weight. When necessary, additional THF was added until a clear solution resulted. Addition of a solution of the salt in THF to CH_2Cl_2 gives a precipitate free of **6**. The absence of free salt in the resultant complex was verified by DSC (absence of the melting point of the free salt in the heating and cooling scans), and in some cases by X-ray scattering experiments.

Results and Discussion

Scheme 1 outlines the synthesis of **6**. All intermediary compounds were synthesized by following procedures available in the literature. The benzo-15-crown-5 **4** was selected as a precursor for the esterification of the benzo-15-crown-5 receptor to the tapered *exo*-receptor since after esterification it maintains an electron donating group on the benzo-15-crown-5 moiety. This functional group does not decrease the complexation ability of the benzo-15-crown-5.[20] The esterification of **4** with **5** was performed under neutral conditions by using a synthetic method detailed in the Experimental section.[12] Under various acidic esterification conditions, cleavage of the benzyl ether groups takes place. The phase behaviour of the self-assembled supramolecule obtained by the complexation of **6** with sodium and potassium triflate was investigated by a combination of techniques consisting of DSC, thermal optical polarized microscopy and X-ray scattering experiments. The phase behaviour of both series of complexes follows the same general trend which is determined by the size of the cation and the amount of salt present in the complex. The size of the anion also affects their phase behaviour, an effect which will be discussed elsewhere.

Figure 1(*a*) presents some representative DSC traces of the second heating scan of the benzoate **6** and of its complexes with sodium triflate ($NaCF_3SO_3$). Compound **6** is crystalline, melting into an isotropic liquid, as also are its complexes containing 0.1 and 0.2 mol of $NaCF_3SO_3$. Although the rate of crystallization of the latter is lower than that of pure **6**, the complex with 0.1 mol of salt still crystallizes on the cooling DSC scan, while the one with 0.2 mol of salt does not crystallize on the cooling scan but crystallizes on the second heating scan (Fig. 1). Complexes of **6** with 0.4 to 1.6 mol of $NaCF_3SO_3$ show crystal meltings only during the first heating scan. During the cooling and subsequent heating scans they do not crystallize. On their first DSC heating scan they exhibit a glass transition, followed by a crystalline phase which melts into a hexagonal columnar (Φ_h) mesophase. All cooling and heating scans show that both the glass transition and the isotropization temperatures increase with the increase in the salt concentration in the complex.

The Φ_h mesophase of the complexes of **6** with $NaCF_3SO_3$ was characterized by thermal optical polarized microscopy and X-ray scattering experiments which will be discussed later. Fig. 1(*b*) shows the dependence of the melting (from both the first and second heating scans), glass transition T_g and Φ_h isotropic transition temperatures obtained from the second DSC heating scan as a function of the $NaCF_3SO_3$:**6** molar ratio. The crystallization, isotropic Φ_h, and glass transition temperatures determined from the first cooling DSC scans are also plotted in the same figure. As expected for a kinetically controlled first-order transition, crystallization occurs at a substantial supercooling. On the other hand the isotropic-Φ_h transition shows only slight supercooling. This is an expected behaviour for a liquid crystalline phase.

Fig. 2(*a*) displays representative DSC traces of the complexes of **6** with KCF_3SO_3 recorded during the second heating scan. The dependence of various phase transition temperatures of **6** and of complexes of **6** with KCF_3SO_3 determined from second heating and first cooling scans as a function of the KCF_2SO_3:**6** molar ratio is plotted in Fig. 2(*b*). Only **6** and its complexes containing 0.1 and 0.2 mol of KCF_2SO_3 are crystalline before the first heating scan; their melting temperatures are also plotted in Fig. 2(*b*). As can be observed from Fig. 2(*a*) during the second and subsequent heating scans, the complex of **6** with as little as 0.1 mol of KCF_3SO_3 is only an isotropic liquid with its glass transition at room temperature. Complexes of **6** with 0.2 and more than 0.2 mol of KCF_3SO_3 exhibit a Φ_h mesophase. For comparison, in the case of the complexes of **6** with

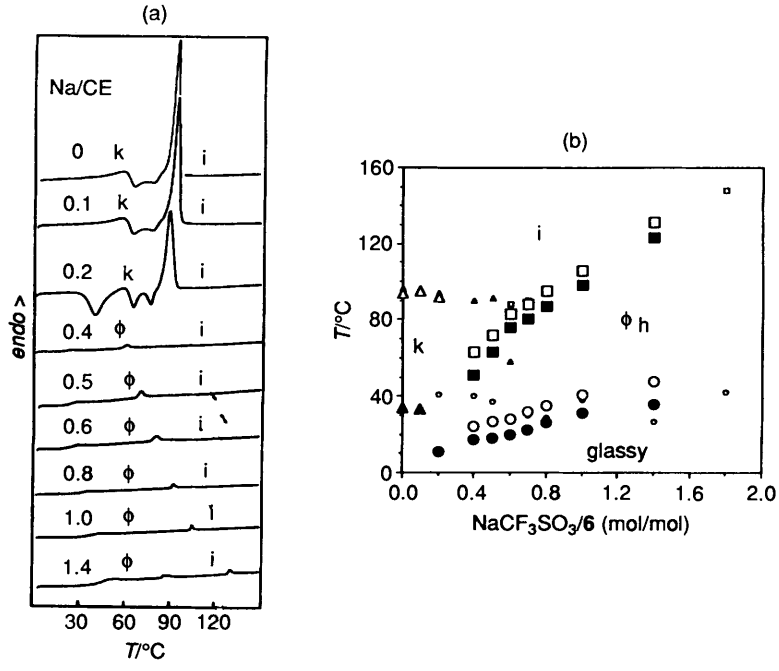

Fig. 1 (*a*) Representative second heating DSC traces (20 °C min^{-1}) of the complexes of **6** with $NaCF_3SO_3$; (*b*) the dependence of the phase transition temperatures of the complexes of **6** with $NaCF_3SO_3$ on the $NaCF_3SO_3$: **6** molar ratio: data from the first heating scan: ○ T_g; △ k–i; □ Φ_h–i; data from the first cooling scan: ● T_g; ▲ k–i; ■ Φ_h–i; data from the second heating scan: ○ T_g; △ k–i; □ Φ_h–i.

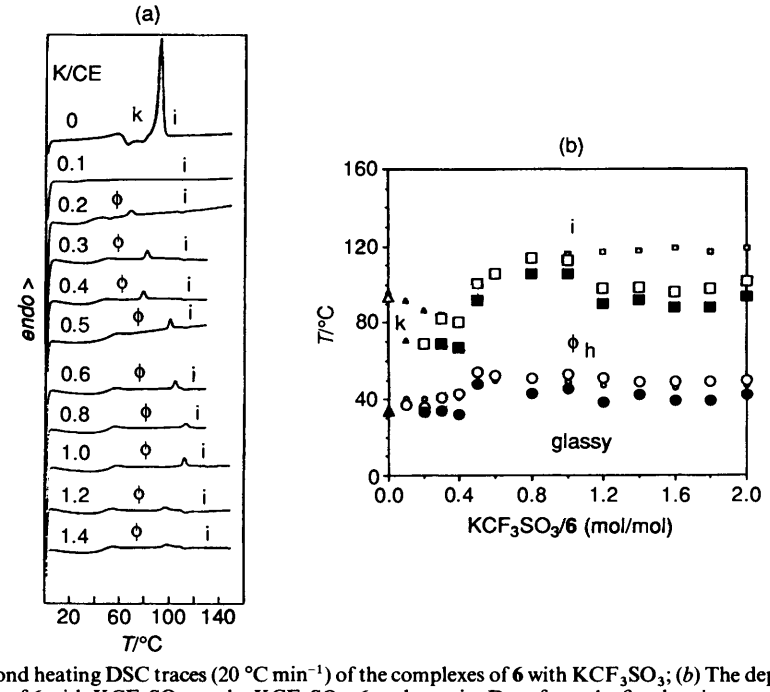

Fig. 2 (*a*) Representative second heating DSC traces (20 °C min^{-1}) of the complexes of **6** with KCF_3SO_3; (*b*) The dependence of the phase transition temperatures of the complexes of **6** with KCF_3SO_3 on the KCF_3SO_3 : **6** molar ratio. Data from the first heating scan: ○ T_g; △ k–i; □ Φ_h–i. Data from the first cooling scan: ● T_g; ▲ k–i; ■ Φ_h–i. Data from the second heating scan: ○ T_g; △ k–i; □ Φ_h–i.

$NaCF_3SO_3$ the formation of the Φ_h mesophase required 0.4 mol of salt. This shows that a salt based on a larger cation induces the formation of the Φ_h mesophase in **6** at lower concentrations. Within experimental error, the enthalpy change associated with the Φ_h isotropic phase transition temperature does not depend on the ratio of **6** to salt but only on the nature of the salt. This value is *ca.* 0.27 ± 0.04 kcal mol^{-1} for the complexes with $NaCF_3SO_3$ and 0.19 ± 0.05 kcal mol^{-1} for the complexes with KCF_3SO_3.

The primary difference between the complexes of benzo-15-crown-5 with sodium and potassium salts consists in their equilibrium constants and their stoichiometry. Benzo-15-crown-5 forms complexes in solution with both sodium and potassium salts.[5f,21] The equilibrium constant of these complexes decreases with increasing cation size. In the solid state, benzo-15-crown-5 forms 1:1 complexes with sodium salts and 2:1 complexes with potassium salts.[5f,22a,b] We have no information about the stoichiometry of the complexes of $NaCF_3SO_3$ and KCF_3SO_3 with the benzo-15-crown-5 group of **6** in the liquid crystalline phase. However, we can speculate that their behaviour should most probably follow the same general trend as in the crystalline phase. Na^+ is complexed within the cavity of the benzo-15-crown-5. However, it prefers to be hexacoordinated and 15-crown-5 provides only five

coordination sites. Therefore, the sixth coordination site of Na^+ is available for interaction with neighbouring receptors. K^+ usually favours hexa- or hepta-coordination. Therefore, a mole of potassium salt is complexed in a sandwich manner by 2 moles of benzo-15-crown-5, and consequently less potassium salt is required to suppress the crystallization of **6** and to generate a Φ_h mesophase from **6**.

It is, however, unexpected that up to 1.8 mol of $NaCF_3SO_3$ per **6** can be accommodated in the mesophase which is generated *via* complexation [Fig. 1(*b*)]. Up to this value both the isotropization and glass transition temperatures of complexes of $NaCF_3SO_3$ with **6** continue to increase. Complexes with higher concentration of $NaCF_3SO_3$ per **6** were not investigated since their isotropization temperature reaches the decomposition temperature. Even the complex of **6** with 1.8 mol of $NaCF_3SO_3$ decomposes above the isotropization temperature and, therefore, Fig. 1(*b*) shows only its data obtained from the first heating scan. This decomposition is most probably due to the Lewis acid character[23] of $NaCF_3SO_3$ which at high temperatures although being deactivated by complexation with the crown ether,[5f] induces the electrophilic cleavage of the benzyl ether groups of **6**. In the case of the complexes of KCF_3SO_3, the maxima of the isotropization and glass transition temperatures are observed at a molar ratio of KCF_3SO_3:**6** = 1.0 [Fig. 2(*b*)]. Above this value the second heating scan shows a slight decrease in the isotropization and glass transition temperatures followed by a plateau. At molar ratios of KCF_3SO_3:**6** > 1.0, a very small amount of free salt may be available in the complex. In addition, some complexed salt seems to be easily released under fast cooling from the isotropic phase. This can be observed by the decrease of the isotropization temperatures observed during the second heating scan for complexes with KCF_3SO_3:**6** > 1.0. Most probably, the benzo-15-crown-5 moieties of these complexes act both as crown ether (*endo*-receptor) and as a solvent in the liquid crystalline state. Therefore, they may dissolve larger amounts of salt than expected based on the behaviour of benzo-15-crown-5 in solution and in crystalline phases.[21,22a,b] However, part of the salt which is not bound by the crown ether cavity forms thermodynamically less stable complexes. This salt is probably released under fast cooling from the isotropic phase.

The size of the cation relative to the size of the crown ether receptor greatly influences the mesophase thermal stability. A comparison of Figs. 1(*b*) and 2(*b*) shows that up to salt:**6** molar ratios of 1:1 a higher mesophase thermal stability is achieved with the complexes of **6** with KCF_3SO_3 *vs.* those with $NaCF_3SO_3$. In the case of complexes of **6** with KCF_3SO_3, 2:1 crown:cation complexes are most probably formed while 1:1 complexes are formed between **6** and $NaCF_3SO_3$. Therefore, complexes of **6** with KCF_3SO_3 exhibit higher isotropization temperatures for the Φ_h mesophase up to concentrations of a 1:1 molar ratio. Above this composition, $NaCF_3SO_3$ continues to be complexed into this supramolecular architecture, while the complexation of KCF_3SO_3 reaches a plateau. Consequently, the isotropization temperature of the complexes of **6** with $NaCF_3SO_3$ continues to increase since the rigidity of the supramolecular assembly increases.[24] At the same time, above a 1:1 molar ratio the complexes of **6** with KCF_3SO_3 maintain a constant isotropization temperature.

Compound **6** and its complexes with 0.6, 0.8 and 1.4 mol of $NaCF_3SO_3$ (*i.e.*, **6**-0.6, **6**-0.8 and **6**-1.4) were characterized by small and wide-angle X-ray scattering; **6** is crystalline at room temperature. Its crystalline phase obtained after fresh recrystallization from solution displays a number of sharp, small and wide-angle reflections. The two most intense small-angle reflections correspond to interplanar spacings of 66.8 and 46.1 Å. On recrystallization from the melt, the same crystalline modification appears as in their crystalline state obtained by crystallization from solution.

Complexes **6**-0.6, **6**-0.8 and **6**-1.4 were first characterized as obtained from the preparation described in the Experimental section. Under these conditions, all show a poorly developed crystalline phase, with a structure different from that of **6**. Reflections are numerous but broad and weak. For all three samples the two most intense small-angle reflections are within ±1 Å of 80 and 48 Å. The 80 Å periodicity corresponds approximately to two molecular lengths of **6**. Once the samples are heated above the melting temperature, the crystalline pattern does not reappear on subsequent cooling. This result is in agreement with that obtained from the DSC data [Fig. 1(*a*, *b*)]. The observed low degrees of crystallinity and crystal perfection in the as prepared complexes of **6** with $NaCF_3SO_3$, as well as the lack of crystallinity developed on cooling from above the melting temperature is consistent with the proximity of the melting and glass transition temperatures ($T_m \approx T_g$ + 30 °C) [Fig. 1(*b*)].

All three complexes containing $NaCF_3SO_3$, *i.e.*, **6**-0.6, **6**-0.8 and **6**-1.4, show the Φ_h phase above the crystal melting temperature. This phase is characterized by the presence of three X-ray reflections in the small-angle range, with spacings in the ratio $d_0:d_1:d_2 = 1:1/\sqrt{3}:1/2$. Only diffuse scattering is observed at wide angles. The measured small-angle spacings are summarized in Table 1. The intensities of the three reflections decrease in the order $d_0 > d_1 > d_2$. Slow formation of columnar monodomains is observed on slow cooling from the isotropic state as is evidenced by the appearance of isolated spotty reflections, particularly in **6**-1.4. The observed interplanar spacings, lattice parameter ($a = 2d^{hex}_{100}/\sqrt{3}$), radius of the cylindrical column ($R = d^{hex}_{100}/\sqrt{3}$), and the side length of the hexagonal column ($S = 2R/\sqrt{3}$) are all reported in Table 1.

In order to derive conclusions about possible molecular arrangement within the columns, molecular models were built of what is believed to be the near minimum-energy conformation of an isolated molecule of **6**. This was based on the conformation of related compounds as determined by crystallographic analyses. Bond lengths, bond angles, and torsion angles were taken from crystallographic data of related compounds as reported in the following publications: torsion angles in aromatic esters,[25a] torsion angles in the planar Ar–O–R group from alkoxy benzoic acids,[25b] torsion angles in the planar Ar–O–R groups of other compounds,[25c] conformation of the uncomplexed benzo-15-crown-5,[25d] and conformation of the complexed benzo-15-crown-5.[25e] The planar conformation of **6** is shown in [Fig. 3(*a*)]. The key dimensions of current interest are only marginally different in the planar conformation from those in the minimum energy state. The following distances are to be compared with the experimental value of *R* (radius of cylindrical column) or *S* (distance from the centre to an edge of a hexagonal column). The distances from the centre of the benzo-15-crown-5 ring to the ends of the three extended aliphatic tails are, respectively: 35.7, 35.4 and 30.4 Å. The overall end-to-end lengths of the molecule (from the end surface of the outermost hydrogen on crown ether ring to the ends of extended aliphatic tails) are respectively: 39.9, 38.9 and 34.5 Å.

In the columnar phase of compounds with tapered molecules of similar shape as the current one, the three aliphatic tails radiate toward the periphery of the column, while the acute apex of the triangular molecule resides near the centre.[26]

A similar arrangement is also expected in the complexes of **6**. Fig. 4 outlines the top and side projections of the three possible supramolecular cylindrical architectures derived from the self-assembly of the complexes of **6**. In the first supramolecular architecture the crown ether cavities are aligned on the central axis of the column, thereby providing a single straight axial

Table 1 Chracterization of the complexes of benzo-15-crown-5 benzoate **6** with sodium triflate by small-angle X-ray scattering

Compound	Na/CE (mol/mol)	d^{hex}_{100} (Å)	d^{hex}_{110} (Å)	d^{hex}_{200} (Å)	$\langle d^{hex}_{100}\rangle$ (Å)	a (Å)	R (Å)	S (Å)	$(R + S)/2$ (Å)
6-0.6	0.6	49.0	28.1	25.1	49.3	56.9	28.5	32.9	30.7
6-0.8	0.8	49.0	28.1	25.0	49.2	56.8	28.5	32.9	30.7
6-1.4	1.4	50.1	28.3	25.4	50.0	57.7	28.9	33.3	31.1
Minimum energy conformation [stacked model; Fig. 4(*a*)]									33.8*
Minimum energy conformation [end-to-end model; four macrocycles, Fig. 4(*b*)]									37.8*
Minimum energy conformation [end-to-end model; five macrocycles, Fig. 4(*c*)]									38.1*

* Calculated from molecular models constructed with Alchemy II from Tripos Assoc.
$\langle d^{hex}_{100}\rangle = (d^{hex}_{100} + d^{hex}_{110} \times \sqrt{3} + d^{hex}_{200} \times 2)/3$, $a = 2\langle d^{hex}_{100}\rangle/\sqrt{3}$, $R = \langle d^{hex}_{100}\rangle/\sqrt{3}$, $S = 2R/\sqrt{3}$.

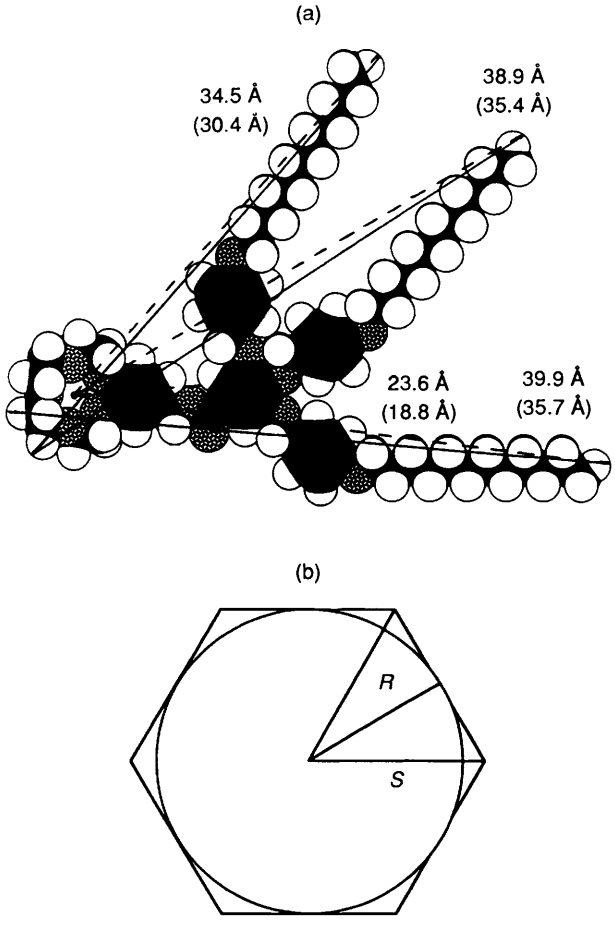

The hexagonal columnar mesophase is characterized by three reflections in the small-angle X-ray scattering pattern with the spacings:

$$d^{hex}_{100} : d^{hex}_{110} : d^{hex}_{200} = 1 : 1/\sqrt{3} : 1/2$$

The hexagonal columnar lattice parameter, a, can be calculated from the d spacings:

$$a = 2\, d^{hex}_{100}/\sqrt{3}$$

The radius (R) of the hard cylinder column, and side length (S) of the hexagonal column unit are related to the lattice parameter, a, through:

$$r = a/2$$
$$S = 2\, R/\sqrt{3}$$

Fig. 3 (*a*) Molecular model of the minimum energy conformation of **6**. Molecular dimensions are measured from the end surface of the outermost hydrogen on the crown ether ring to the ends of the extended aliphatic tails. Molecular dimensions in parentheses are measured from the centre of the crown ether ring to the ends of the aliphatic tails; (*b*) characterization of the hexagonal columnar (Φ_h) mesophase by small-angle X-ray scattering.

channel. This proposition does not seem reasonable by the current experimental results. The experimentally determined average distance from the centre of the column cavity to the extended tail ends [$(R + S)/2 = 30.7$ Å] (Table 1) is only slightly lower than the measured distance from the centre to the edge of the column (33.8 Å) [see Fig. 4(*b*) and Table 1]. However, due to the conformational melting of the aliphatic tails, the experimentally measured column radii should fall significantly short of the radii based on the extended molecular lengths.[25] If it is assumed that the difference between the experimentally determined column radius and the measured radius of the extended conformation model is due only to flexibility of the alkyl trails, the extent of the alkyl tail shrinkage can be determined as follows:

$$\%\ \text{shrinkage} = \frac{R_{ext.} - R_{exp.}}{R_{ext.} - R_{core}} \times 100$$

$R_{ext.}$ = average measured radius from extended conformation model [Fig. 3(*a*)], $R_{exp.}$ = average radius determined experimentally (Table 1) and R_{core} = radius of rigid aromatic core [Fig. 3(*a*)]

For the case where the crown ether rings are centred in the column [Fig. 4(*a*)], the experimental value corresponds to an alkyl tail shrinkage of 21%. Previous work in our laboratory[26] has, in fact, shown a shrinkage of as much as 55% for similar compounds. Thus, if the crown ether ring was centrally placed, the size of the remaining part of the molecule in its realistic non-extended conformation would not be sufficient to reach the edge of the column. In addition, the side projection [Fig. 4(*a*) bottom] reveals a significant amount of empty space which cannot be filled by the low amount of melted alkyl chains.

If, on the other hand, four macrocycles were placed side by side within the column core [Fig. 4(*b*)], then the relevant molecular dimension, to be compared with R and S values, becomes the end-to-end distance of **6**. This averaged distance, 37.8 Å, is 7.1 Å larger than the 30.7 Å average centre-to-edge dimension of the column [$(R + S)/2$]. This 7.1 Å difference represents an alkyl tail shrinkage of 50%, and is well accounted for by the behaviour of other similar compounds.[26a] Furthermore, the side view in Fig. 4(*b*) shows a good space-filling ability of the side-by-side arrangement of macrocycles, as opposed to that of the stacked arrangement in Fig. 4(*a*).

Viable arrangements with five macrocycles placed side-by-side can also be envisaged, although some departure from coplanarity would appear to be required [see Fig. 4(*c*)]. Fig 4(*c*) displays the top and side projections of the supramolecular column derived from five macrocycles placed side-by-side within the column core. Out-of-plane rotation of the crown ether group about the CH_2–(Ph–crown ether) bond allows a more efficient packing of the space between the molecules of **6**. The arrangement of five molecules with this conformation in a

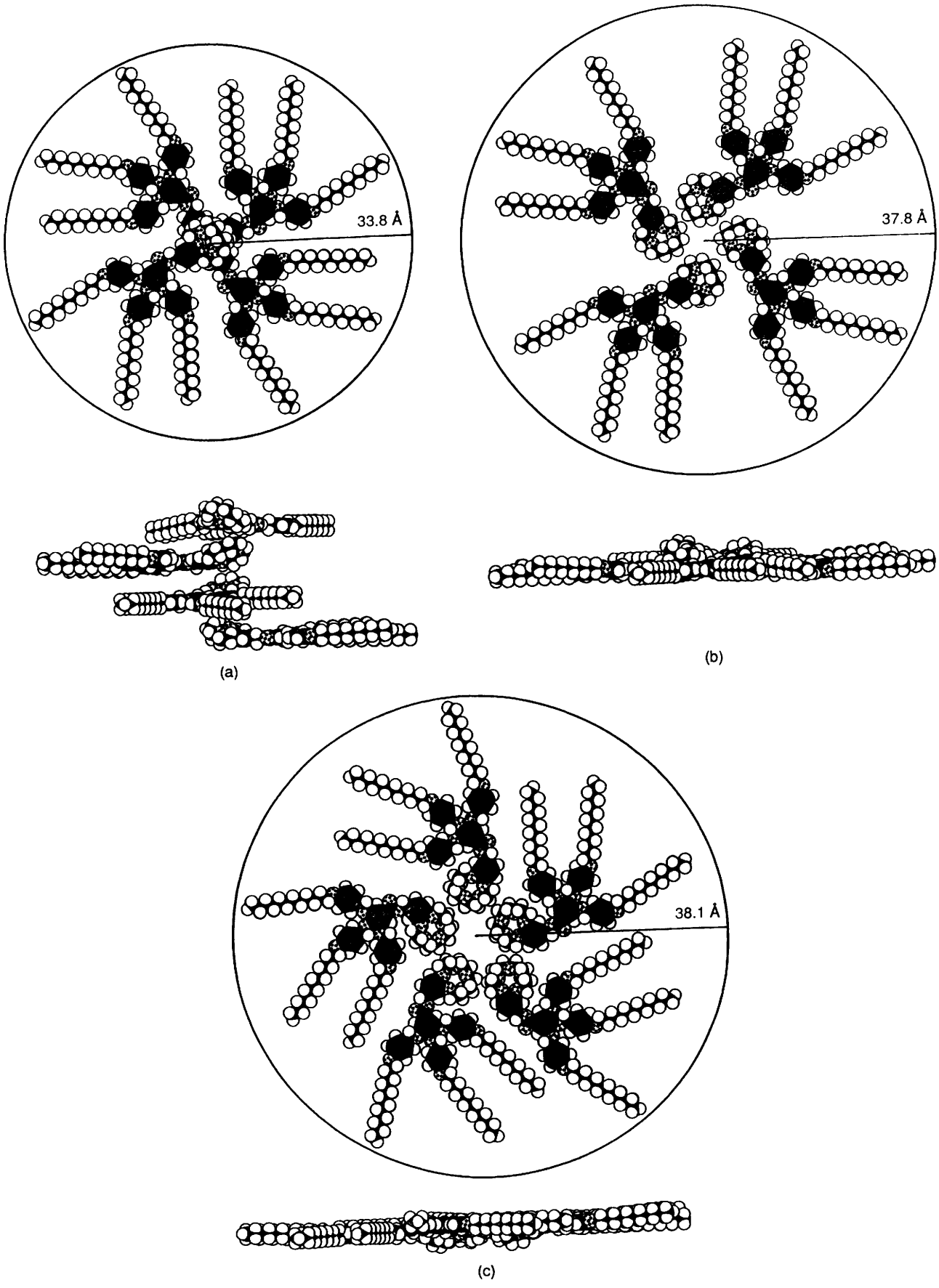

Fig. 4 (*a*) Top (upper) and side projections (lower) of a 'stacked' supramolecular cylindrical architecture derived from molecular models of **6**. (*b*) Top (upper) and side (lower) projections of an 'end-to-end' supramolecular cylindrical architecture containing four macrocycles derived from molecular models of **6**. (*c*) Top (upper) and side (lower) projections of an 'end-to-end' supramolecular cylindrical architecture containing five macrocycles derived from molecular models of **6**.

circular arrangement requires the formation of a void in the centre of the column to prevent the overlap of atoms. In this model the relevant molecular dimension to be compared with R and S values is the distance from the centre of the column to the ends of the extended alkyl tails. This distance of 38.1 Å is 7.4 Å larger than the corresponding 30.7 Å centre-to-edge dimension of the column measured experimentally. Furthermore, the corresponding rigid aromatic core radius of 23.8 Å requires an alkyl tail shrinkage of 52%, which is also in good agreement with previous results.

The X-ray density of the self-assembled supramolecular architecture generated *via* the complexation of **6** can be calculated based on the following equation which uses the volume of a unit hexagonal prism of known base area and an assumed height t:

$$\rho = \frac{2n\mathrm{M}}{3\sqrt{3}N_{\mathrm{A}}S^2t}.$$

Here M is the molecular weight of **6** weight averaged for 0.6 mol of $NaCF_3SO_3$ per **6** (1191 daltons), n is the number of molecules of **6** in a cross section, N_A is $6.022\,045 \times 10^{23}$ mol^{-1} (Avogadro's number). In the case of models from Fig. 4(*b*) and 4(*c*), t is taken as the average spacing between adjacent benzene rings in the direction of the column axis as reported in the literature (3.74 Å)[27] and S is the experimental value of the distance from the column centre to the hexagon vertex [see Fig. 3(*b*), Table 1]. Based on these values the arrangement shown in Fig. 4(*a*) but with melted alkyl tails has a four times larger t value than that of Fig. 4(*b*), and provides a calculated density of 0.19 g cm^{-3}. Therefore, this value excludes the model from Fig. 4(*a*). Likewise, the arrangements in Fig. 4(*b*) (n = 4) and 4(*c*) (n = 5) with melted alkyl tails have densities of 0.75 and 0.94 g cm^{-3}, respectively. The density of **6**-0.6 was measured using a density gradient column (water–ethylene glycol) and is 1.09 g cm^{-3}. This value requires 5.8 molecules of **6** per column stratum. This number suggests that most probably, the average molecular spacing in the direction of the column axis t is > 3.74 Å.

Table 1 shows the dependence of the column radius on the $NaCF_3SO_3$:**6** molar ratio. Within the experimental accuracy, the column radius R is seen to remain constant. Although a slight decrease in radius is observed, it is not experimentally significant. Since sodium is complexed within the cavity of the benzo-15-crown-5 unit, and potassium forms a sandwich between two benzo-15-crown-5 groups,[5f] there should not be a significant difference between the diameters of the supramolecular complexes of **6** with various salt contents. This behaviour is contrasted with that observed for similar compounds containing oligooxyethylene side groups in the place of benzo-15-crown-5 groups, where R depends considerably on salt concentration.[28]

On the optical polarized microscope, the Φ_h mesophases of the complexes of **6** with $NaCF_3SO_3$ and KCF_3SO_3 exhibit a fan shaped texture which is representative for a Φ_h mesophase obtained with discotic mesogens. A representative texture is presented in Fig. 5.

In spite of the above conclusions about the column structure, we notice that the unfeasibility of the central channel or tube model [Fig. 4(*a*)] does not preclude the possibility of more or less continuous macrocyclic channels propagating through the column core [Fig. 4(*b*, *c*)]. One can envisage either five or more parallel linear channels extending side by side. Alternatively, macrocycle planes may be tilted, resulting concievably in multiple-stranded helical or undulated channels. However, such proposals remain highly speculative at present.

As with all column-forming compounds based on similar tapered architectures,[26] and in common with most discotics, X-ray scattering patterns of the isotropic phase are characterized by a diffuse scattering ring in the low angle region (at 46 Å in the case of **6**-0.6), in addition to the wide-angle halo in the 4.5 Å region. The intense diffuse low-angle peak is always centred close to the position of the 100 reflection of the hexagonal columnar lattice and indicates the existence of strong column-like fluctations of the type which becomes long-range below the isotropic-Φ_h transition. Therefore, in the isotropic phase, the complexes of **6** exist as self-assembled discs which are likely to stack in short distorted columns. However, these columns lack the long range order of the Φ_h phase.

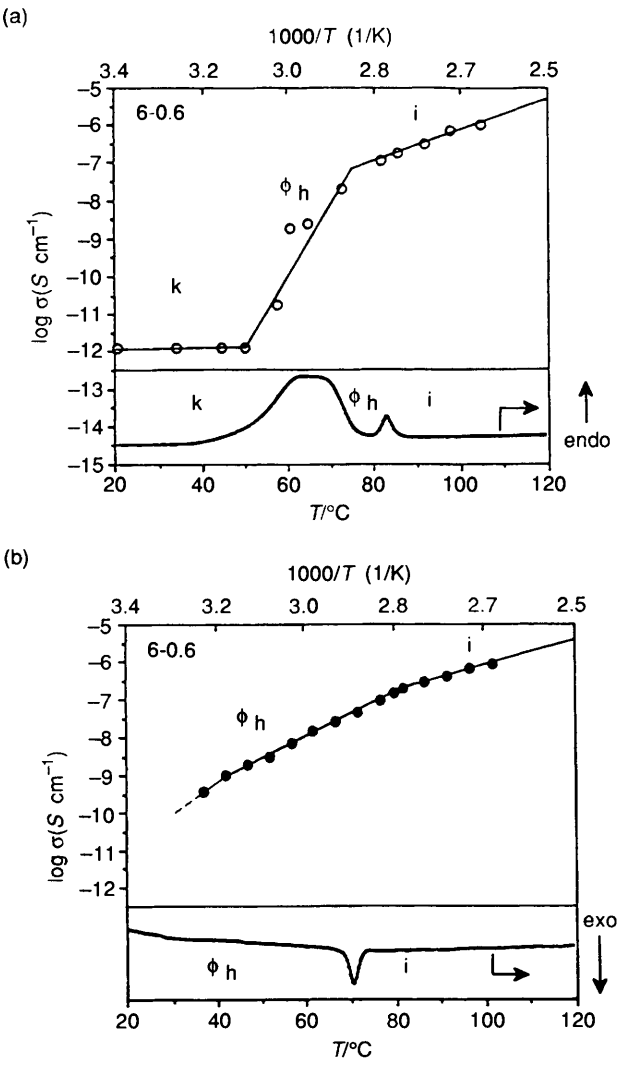

Fig. 6 (*a*) The dependence of logσ (S cm^{-1}) *vs.* T(°C) and $1/T$ (1/K) during the first heating scan of the crystalline **6**-0.6 complex (upper part) and its corresponding DSC scan (20 °C min^{-1}); (*b*) the dependence of logσ (S cm^{-1}) *vs.* T(°C) and $1/T$ (1/K) obtained during cooling from the isotropic phase of **6**-0.6 complex (upper part) and its DSC scan (20 °C min^{-1}).

The mechanism of self-assembly of **6** *via* complexation with $NaCF_3SO_3$ and KCF_3SO_3 resembles that of the self-assembly of the tobacco mosaic virus (TMV) from its constituent proteins in the absence of ribonucleic acid (RNA).[3a,b,26c,28] TMV is a virus consisting of 2130 identical protein subunits and a strand of RNA. The information required for the self-assembly of TMV is available in its constituent parts. Under low pH conditions the tapered protein subunits self-assemble into a TMV even in the absence of RNA. The main driving force for the self-assembly of TMV in the absence of RNA is provided in this case by the *exo*-recognition of the tapered shape of its protein subunits. In the presence of RNA addition *endo*-recognition

Fig. 5 Representative optical polarized micrograph of the texture exhibited by the columnar hexagonal (Φ_h) mesophase of the complex of **6** with $NaCF_3SO_3$ (1:1 molar ratio) at 103 °C on the cooling scan (20 °C min^{-1}).

[facing p. 1418

between the RNA and the protein subunits is provided.[28] As observed from Figs. 3(*a*), (*b*) and 4, **6** has a tapered shape. *exo*-Recognition of the tapered shapes of **6** and *endo*-recognition provided by the *endo*-crown ether receptor upon complexation are responsible for the self-assembly of **6**.

Fig. 6(*a*) presents the dependence of logσ *vs.* T(°C) and $1/T$(1/K), and the corresponding DSC scan (20 °C min^{-1}), both recorded during the first heating scan of **6**-0.6 while Fig. 6(*b*) describes the same data collected from the cooling scans. As observed from Fig. 6 the onset of the transition temperatures determined from DSC scans are *ca.* 5 °C higher on heating and *ca.* 10 °C lower on cooling than the corresponding transitions determined from the DC conductivity measurements. The higher difference from the cooling scan is due to the difference between the cooling rates used in the two experiments. Extrapolation of the phase transition temperatures from the cooling DSC experiment to zero rate shifts these two sets of data to *ca.* 5 °C from each other. Since the heating scan in Fig. 6(*a*) is the first scan, the sample is crystalline; hence very low conductivity is measured at temperatures below the onset of the melting point. During the melting process, a large increase in conductivity is observed. The slope of the dependence σ *vs.* T changes at the Φ_h-isotropic phase transition. On cooling from the isotropic melt at the rate employed, crystallization is prevented, so the difference between the isotropic and columnar phase can be observed even more clearly than on the heating scan [Fig. 6(*b*)]. DC conductivity in the range of 10^{-6} and 10^{-7} S cm^{-1}, as observed in the isotropic and columnar phases, are typical for ionic conductors.[30] In the range of the supercooled columnar phase and as glass transition temperature is approached, conductivity drops into the range of insulators. Activation energies for the conduction process are 20 kcal mol^{-1} for the isotropic, and 28 kcal mol^{-1} for the columnar phase. There is only a very small jump in σ at the isotropic-Φ_h transition; otherwise, regarding conductivity, the two phases behave very similarly. In view of the reduced motion of the supramolecular cylinders in the Φ_h phase relative to the isotropic melt, the similarity in σ suggests that ion migration between molecules is at least partially responsible for charge transport. On the optical polarized microscope we observed a significantly higher viscosity in the Φ_h phase *vs.* isotropic phase. In the case of the Φ_h phase, the channel-like supramolecular arrangement proposed here on the basis of X-ray data appears to be consistent with ion migration through the channel since crown ether groups positioned along the column axes would provide a continuous passage for this form of charge transport. Unfortunately, so far we have not succeeded in preparing orientated samples which would allow separate measurements of conductivities parallel and perpendicular to the column axis. Under these conditions, our conductivity measurement may reflect the rate-limiting step which most probably is hopping of the ions from column to column and, therefore, conductivity values could be lower and activation energies higher than the corresponding intracolumnar values. Therefore, a comparison of these activation energies with those characteristic for the channel and carrier mechanisms[8a] is not meaningful at the present time. Work in this direction is currently in progress.

The self-assembly of **6** in the presence of other metal salts based on different cations and anions as well as a detailed study of the transport through these supramolecular channels are under investigation. The formation of conventional disc-like and rod-like supramolecular mesogens *via* molecular recognition processes generated by means of metal complexes[31,32] and hydrogen bonding[31,33] has already been demonstrated. However, the self-assembling concept elaborated in this publication is different from previously reported ones since it generates a complex supramolecular cylindrical architecture. In a forthcoming publication we shall report on the use of other *endo*- and *exo*-receptors in the molecular engineering of supramolecular self-assembled TMV-like structures *via* a combination of molecular and supramolecular chemistry.

Acknowledgements

Financial support by the National Science Foundation (DMR-92-06781), and a NATO travelling grant are gratefully acknowledged.

References

1 (*a*) J. M. Lehn, *Angew. Chem., Int. Ed. Engl.*, 1988, **27**, 89; (*b*) D. J. Cram, *Angew. Chem., Int. Ed. Engl.*, 1988, **27**, 1009; (*c*) C. J. Pedersen, *Angew. Chem., Int. Ed. Engl.*, 1988, **27**, 1021.

2 (*a*) J. M. Lehn, *Angew. Chem., Int. Ed. Engl.*, 1990, **29**, 1304; (*b*) H. J. Schneider, *Angew. Chem., Int. Ed. Engl.*, 1991, **30**, 1417.

3 (*a*) J. S. Lindsey, *New J. Chem.*, 1991, **15**, 153; (*b*) G. M. Whitesides, J. P. Mathias and C. T. Seto, *Science*, 1991, **254**, 1312; (*c*) H. J. Schneider and H. Durr, eds. *Frontiers in Supramolecular Organic Chemistry and Photochemistry*, VCH, New York, 1991; (*d*) F. Vogtle, *Supramolecular Chemistry*, John Wiley & Sons, New York, 1992; for a series of books on supramolecular chemistry, see: (*e*) J. F. Stoddart, series ed., *Monographs in Supramolecular Chemistry*, Royal Soc. Chem., Cambridge, 1991; (*f*) G. W. Gokel, series ed., *Advances in Supramolecular Chemistry*, JAI Press, London, vol. 1, 1990 and vol. 2, 1992.

4 (*a*) J. Rebek Jr., *Angew. Chem., Int. Ed. Engl.*, 1990, **29**, 245; (*b*) D. Philip and J. F. Stoddart, *Synlett*, 1991, 445.

5 (*a*) W. D. Stein, *Channels, Carriers, and Pumps. An Introduction to Membrane Transport*, Academic Press, New York, 1990; (*b*) B. Hille, *Ionic Channels of Excitable Membranes*, Sinauer Assoc. Inc., Sunderland, MA, 1984; (*c*) R. D. Fox Jr. and F. M. Richards, *Nature*, 1982, **25**, 325; (*d*) D. W. Urry, *Top. Curr. Chem.*, 1985, **128**, 175; (*e*) J. K. Aronson, *Biochem. Pharmacol.*, 1992, **42**, 11; (*f*) O. H. Petersen, *Biochem. Pharmacol.*, 1992, **42**, 1; (*g*) G. W. Gokel, *Crown Ethers and Cryptands*, in *Monographs in Supramolecular Chemistry*, J. F. Stoddart, series ed., Royal Soc. Chem., Cambridge, 1991.

6 (*a*) B. A. Wallace, *Biophys. J.*, 1986, **49**, 295; (*b*) B. A. Wallace, *Ann. Rev. Biophys. Chem.*, 1990, **19**, 127; (*c*) M. C. Bano, L. Braco and C. Abad., *Biochemistry*, 1991, **30**, 886; (*d*) A. S. Cifu, R. E. Koeppe II and O. S. Anderson, *Biophys. J.*, 1992, **61**, 189.

7 (*a*) M. J. Pregel, L. Jullien and J. M. Lehn, *Angew. Chem., Int. Ed. Engl.*, 1992, **31**, 1637 and references cited therein; (*b*) A. Nakano, Q. Xie, J. V. Mallen, L. Echegoyen and G. W. Gokel, *J. Am. Chem. Soc.*, 1990, **112**, 1287; (*c*) G. W. Gokel, *Chem. Soc. Rev.*, 1992, 39; (*d*) G. W. Gokel, *CIBA Foundation Symposia*, 1992, **158**, 23; (*e*) J. G. Neevel and R. J. M. Nolte, *Tetrahedron Lett.*, 1984, **25**, 2263; (*f*) U. F. Kragten, M. F. M. Roks and R. J. M. Nolte, *J. Chem. Soc., Chem. Commun.*, 1985, 1275; (*g*) I. Tabushi, Y. Kuroda and K. Yokota, *Tetrahedron Lett.*, 1982, **23**, 4601; (*h*) B. M. Novak and R. H. Grubbs, *J. Am. Chem. Soc.*, 1988, **110**, 960; (*i*) B. Tümmler, G. Maass, F. Vögtle, H. Sieger, U. Heimann and E. Weber, *J. Am. Chem. Soc.*, 1979, **101**, 2588 and references cited therein.

8 (*a*) S. Shinkai, G. X. He, T. Matsuda, K. Shimamoto, N. Nakashima and O. Manabe, *J. Polym. Sci. Part C: Polym. Lett.*, 1989, **27**, 209 and references cited therein; (*b*) K. Kimura, T. Suzuki and M. Yokogama, *J. Phys. Chem.*, 1990, **94**, 6090.

9 (*a*) S. Shinkai, T. Nishi, A. Ikeda, T. Matsuda, K. Shimamoto and O. Manabe, *J. Chem. Soc., Chem. Commun.*, 1990, 303; (*b*) G. X. He, F. Wada, K. Kikukawa, S. Shinkai and T. Matsuda, *J. Org. Chem.*, 1990, **55**, 541 and 548; (*c*) T. Nishi, A. Ikeda, T. Matsuda and S. Shinkai, *J. Chem. Soc., Chem. Commun.*, 1991, 339; (*d*) S. Shinkai, T. Nishi and T. Matsuda, *Chem. Lett.*, 1991, 437; (*e*) V. Percec and R. Rodenhouse, *Macromolecules*, 1989, **22**, 4043 and 4408; (*f*) V. Percec and R. Rodenhouse, *J. Polym. Sci. Part A: Polym. Chem.*, 1991, **29**, 15; (*g*) G. Ungar, V. Percec and R. Rodenhouse, *Macromolecules*, 1991, **29**, 1996; (*h*) R. Rodenhouse, V. Percec and A. E. Feiring, *J. Polym. Sci. Part C: Polym. Lett.*, 1990, **28**, 345; (*i*) V. Percec and R. Rodenhouse, *Adv. Mater.*, 1991, **1**, 1015 and references cited therein; (*j*) G. H. Hsiue, J. S. Wen and C. S. Hsu, *Makromol. Chem.*, 1991, **192**, 2243; (*k*) V. Percec, G. Johansson and R. Rodenhouse, *Macromolecules*, 1992, **25**, 2563; *J. Mater. Chem.*, 1993, **3**, 83.

10 (*a*) J. M. Lehn, J. Malthete and A. M. Levelut, *J. Chem. Soc., Chem. Commun.*, 1985, 1794; (*b*) A. Liebmann, C. Mertesdorf, T. Plesnivy, H. Ringsdorf and J. H. Wendorff, *Angew. Chem., Int. Ed. Engl.*, 1991, **30**, 1375 and references cited therein; (*c*) G. Lattermann, S. Schmidt,

R. Kleppinger and J. H. Wendorff, *Adv. Mater.*, 1992, **4**, 30; (*d*) D. Tatarsky, S. Schmidt, R. Kleppinger and J. H. Wendorff, *Adv. Mater.*, 1992, **4**, 30; (*d*) D. Tatarsky, K. Banerjee and W. T. Ford, *Chem. Mater.*, 1990, **2**, 138; (*e*) S. H. J. Idziak, N. C. Maliszewskyj, A. Heiney, J. P. McCauley, A. Sprengeler and A. B. Smith III, *J. Am. Chem. Soc.*, 1991, **113**, 7666; (*f*) S. H. J. Idziak, N. C. Maliszewskyj, G. B. M. Vaughan, A. Heiney, C. Mertesdorf, H. Ringsdorf, J. P. McCauley and A. B. Smith III, *J. Chem. Soc., Chem. Commun.*, 1992, 98.

11 (*a*) C. Sirlin, L. Bosio, J. Simon, V. Ahsen, E. Yilmazer and O. Bekaroglu, *Chem. Phys. Lett.*, 1987, **139**, 362; (*b*) J. Simon and C. Sirlin, *Pure Appl. Chem.*, 1989, **61**, 1625; (*c*) J. Simon, M. K. Engel and C. Soulie, *New J. Chem.*, 1992, **16**, 287.

12 J. S. Moore and S. I. Stupp, *Macromolecules*, 1990, **23**, 65.

13 T. Gramstad and R. N. Haszeldine, *J. Chem. Soc.*, 1956, 173.

14 C. J. Pedersen, *J. Am. Chem. Soc.*, 1967, **89**, 7017.

15 (*a*) A. G. Talma, H. Van Vossen, E. J. R. Sudholter, J. Van Eerden and D. N. Reinhoudt, *Synthesis*, 1986, 680; (*b*) F. Wada, R. Arata, T. Goto, K. Kikukawa and T. Matsuda, *Bull. Chem. Soc. Jpn.*, 1980, **53**, 2061.

16 M. Bourgoin, K. H. Wong, J. Y. Hui and J. Smid, *J. Am. Chem. Soc.*, 1975, **97**, 3462.

17 N. M. Yoon, C. S. Pak, H. C. Brown, S. Krishnamurthy and T. Stocky, *J. Org. Chem.*, 1973, **38**, 2786.

18 E. M. Hyde, B. L. Shaw and I. Shepherd, *J. Chem. Soc., Dalton Trans.*, 1978, 1696.

19 (*a*) J. Malthete, N. Tinh and A. M. Levelut, *J. Chem. Soc., Chem. Commun.*, 1986, 1548; (*b*) V. Percec and J. Heck, *J. Polym. Sci. Part A: Polym. Chem.*, 1991, **29**, 591.

20 R. Ungaro, B. El Haj and J. Smid, *J. Am. Chem. Soc.*, 1976, **98**, 5198.

21 Y. Takeda, *Top. Curr. Chem.*, 1984, **121**, 1.

22 (*a*) M. A. Bush and M. R. Truter, *J. Chem. Soc., Perkin Trans. 2*, 1972, 341; (*b*) R. Mallinson and M. R. Truter, *J. Chem. Soc., Perkin Trans. 2*, 1972, 1818.

23 (*a*) J. Collomb, P. Arlaud, A. Gandini and H. Cheradame, in *Cationic Polymerization and Related Processes*, ed. E. J. Goethals, Academic Press, New York, 1984, 49 and references cited therein; (*b*) Y. Eckstein and P. Dreyfuss, *J. Inorg. Nucl. Chem.*, 1981, **43**, 23; (*c*) A. Loupy and B. Tchoubar, *Salt Effects in Organic and Organometallic Chemistry*, VCH, Weinheim, 1992, 2.

24 (*a*) V. Percec and A. Keller, *Macromolecules*, 1990, **23**, 4347; (*b*) A. Keller, G. Ungar and V. Percec, *Advances in Liquid Crystalline Polymers*, eds. R. A. Weiss and C. K. Ober, ACS Symposium Series, 435, Washington, DC, 1990, 308.

25 (*a*) P. J. Flory and J. P. Hummel, *Macromolecules*, 1980, **13**, 479; (*b*) R. F. Bryan, P. Hartley and R. W. Miller, *Mol. Cryst. Liq. Cryst.*, 1980, **62**, 311; (*c*) J. Shashidhara-Prasad, *Acta Crystallogr., Sect. B*, 1979, **35**, 1404; H. G. Wiedemann, J. Grebowitz and B. Wunderlich, *Mol. Cryst. Liq. Cryst.*, 1986, **140**, 219; M. Cotrait, P. Marsau and M. Pesquer, *Acta Crystallogr., Sect. B*, 1979, **35**, 1102; R. W. G. Wyckoff, *Crystal Structures*, Interscience, New York, 2nd edn., 1963, vol. 5, ch. XIV and Fig. XIV, 20; (*d*) I. R. Hanson, *Acta Crystallogr., Sect. B*, 1978, **34**, 1026; (*e*) M. A. Bush and M. R. Truter, *J. Chem. Soc., Perkin Trans. 2*, 1972, 341; E. Weber and M. Czugler, *Inorg. Chim. Acta*, 1982, **61**, 33; G. Ungar, V. Percec and R. Rodenhouse, *Macromolecules*, 1991, **24**, 1996.

26 (*a*) V. Percec, G. Ungar and J. Heck, *Macromolecules*, 1991, **24**, 4957; (*b*) V. Percec, J. Heck, M. Lee, H. Blackwell, G. Ungar and A. Castillo, *J. Mater. Chem.*, 1992, **2**, 931; (*c*) V. Percec, J. Heck, M. Lee, G. Ungar and A. Castillo, *J. Mater. Chem.*, 1992, **2**, 1033.

27 C. R. Safinya, K. S. Liang, W. A. Varady, N. A. Clark and G. Anderson, *Phys. Rev. Lett.*, 1984, **53**, 1172.

28 A. Klug, *Angew. Chem., Int. Ed. Engl.*, 1982, **22**, 565.

29 V. Percec, J. Heck, H. Blackwell, F. Falkenberg and G. Ungar, unpublished work.

30 F. M. Gray, *Solid Polymer Electrolites. Fundamentals and Technological Applications*, VCH Publ., New York, 1991.

31 For brief reviews on supramolecular chemistry and liquid crystallinity see: (*a*) V. Percec and D. Tomazos, in *Polymerization in Liquid Crystalline Media*, ed. C. M. Paleos, Gordon and Breach, New York, 1992, p. 1–104; (*b*) V. Percec and D. Tomazos, in *Comprehensive Polymer Science, Suppl. Vol. 1*, ed. G. Allen, Pergamon Press, Oxford, 1992, p. 299–383.

32 (*a*) For a review on metallomesogens see: A. M. Giroud-Godquin and P. M. Maitlis, *Angew. Chem., Int. Ed. Engl.*, 1991, **30**, 375; (*b*) For a recent publication see M. J. Baena, P. Espinet, M. C. Leguerica and A. M. Levelut, *J. Am. Chem. Soc.*, 1992, **114**, 4182.

33 For recent representative publications on self-assembling of disc-like and rod-like mesogens *via* hydrogen bonding see: (*a*) C. Fonquey, J. M. Lehn and A. M. Levelut, *Adv. Mater.*, 1990, **2**, 254; (*b*) M. J. Brienne, J. Gabard, J. M. Lehn and I. Stibor, *J. Chem. Soc., Chem. Commun.*, 1989, 1868; (*b*) U. Kumar, T. Kato and J. M. J. Frechet, *J. Am. Chem. Soc.*, 1992, **114**, 6630, and references cited therein.

Paper 3/01377D
Received 9*th March* 1993
Accepted 26*th March* 1993